HHS Public Access

Author manuscript

Methods. Author manuscript; available in PMC 2019 April 01.

Published in final edited form as:

Methods. 2018 April 01; 138-139: 76–84. doi:10.1016/j.ymeth.2017.12.020.

Enhanced Spectral Density Mapping through Combined Multiple-Field Deuterium $^{13}CH_2D$ Methyl Spin Relaxation NMR Spectroscopy

Andrew Hsu[1], **Paul A. O'Brien**[2], **Shibani Bhattacharya**[3], **Mark Rance**[4], and **Arthur G. Palmer III**[2]

[1]Department of Chemistry, Columbia University, 3000 Broadway, New York, NY 10027

[2]Department of Biochemistry and Molecular Biophysics, Columbia University Medical Center, 650 West 168th Street, New York, NY 10032

[3]New York Structural Biology Center, 89 Convent Avenue, New York, NY 10027

[4]Department of Molecular Genetics, Biochemistry, and Microbiology, University of Cincinnati College of Medicine, 231 Albert Sabin Way, Cincinnati, OH 45267

Abstract

Quadrupolar relaxation of ^2H (D) nuclear spins is a powerful probe of conformational dynamics in biological macromolecules. Deuterium relaxation rate constants are determined by the spectral density function for reorientation of the C-D bond vector at zero, single-quantum, and doublequantum ^2H frequencies. In the present work, ^2H relaxation rate constants were measured for an *E. coli* ribonuclease H [U-^2H, ^{15}N] ILV-[$^{13}CH_2D$] sample using 400, 500, 800, and 900 MHz NMR spectrometers and analyzed by three approaches to determine spectral density values. First, data recorded at each static magnetic field were analyzed independently. Second, data recorded at 400 and 800 MHz were analyzed jointly and data recorded at other fields were analyzed independently. Third, data recorded at 400 and 500 MHz were interpolated to 450 MHz, and the resulting two pairs of data, corresponding to 400 MHz/800 MHz and 450 MHz/900 MHz, were analyzed jointly. The second and third approaches rely on the identity between the double quantum frequency at the lower field and the single quantum frequency at the higher field. Spectral density values for 32 of the 48 resolvable ILV methyl resonances were fit by the Lipari-Szabo model-free formalism and used to validate the three methods. The three spectral density mapping methods performed equally well in cross validation with data recorded at 700 MHz. However, the third method yielded approximately 10–15% more precise estimates of model-free parameters and consequently provides a general strategy for analysis of ^2H spin relaxation data in biological macromolecules.

Graphical abstract

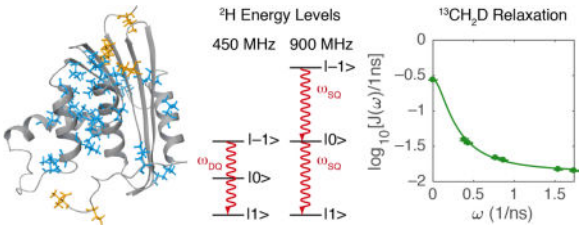

Keywords

protein dynamics; spectral density mapping; deuterium relaxation; ribonuclease H

1. Introduction

Intramolecular dynamics of proteins and other biological macromolecules increasingly are recognized as playing important roles in function, including allostery, catalysis, molecular recognition, regulation, and signaling [1–3]. Spin relaxation in NMR spectroscopy is a powerful probe of dynamics and kinetics of biological macromolecules with atomic resolution and over a broad range of time scales [4, 5]. Methods and applications have been reported for ^{1}H, ^{2}H, ^{13}C, and ^{15}N nuclei in proteins and nucleic acids [5, 6]. Deuterium (^{2}H or D) relaxation offers advantages when compared with other nuclei in characterizing the dynamic properties of molecules in solution. First, ^{2}H relaxation is dominated by the quadrupolar mechanism, and contributions from other mechanisms such as chemical shift anisotropy (CSA) and chemical exchange are negligible in comparison. Second, the quadrupolar Hamiltonian is axially symmetric and the principal axis is oriented along the carbon-deuterium bond, which simplifies interpretation of relaxation measurements. In contrast, CSA tensors may be rhombic and have principal axes systems that are rotated relative to convenient reference directions.

Kay and coworkers established methods for measuring relaxation of ^{2}H spins in CH_2D methyl group isotopomers in proteins in solution [7, 8]. These methods subsequently were extended to CD, CHD, and CHD_2 moieties in proteins [9, 10] and CD and CHD moieties in RNA [11, 12]. The rate constants R_1, $R_{1\rho}$, R_Q, R_{AP}, and R_{DQ} describe ^{2}H quadrupolar relaxation of longitudinal magnetization (D_z), transverse magnetization (D^+), quadrupolar order ($3D_z^2 - 2$), antiphase coherence ($D^+D_z + D_zD^+$), and double-quantum coherence (D^{+2}), respectively. At a given static magnetic field strength, the relaxation of the density operator is dependent on the values of the spectral density function, $J(\omega)$, at three frequencies: 0, ω_D, and $2\omega_D$, in which ω_D is the ^{2}H Larmor frequency. Because the five relaxation rate constants measured for the deuterium spin are defined by the spectral density functions of three deuterium frequencies, the spectral density values can be determined if three or more relaxation rate constants are measured. Inversion of the relaxation equations to obtain the values of the spectral density function is called spectral density mapping [13, 14]

The present work examines three approaches for spectral density mapping when relaxation data have been acquired at more than one static magnetic field strength. In the simplest approach, termed the *independent method*, each static magnetic field is treated

independently [7, 8, 15]. If data sets are obtained using two NMR spectrometers whose static magnetic field differ by a factor of two, then the double-quantum frequency, $2\omega_D$, at the lower field is equal to the single quantum frequency at the higher field [8, 16]. In this case, the relaxation data recorded at the two static magnetic fields can be analyzed simultaneously to obtain $J(\omega)$ at frequencies of 0, ω_D, $2\omega_D$, $4\omega_D$, in which ω_D is the Larmor frequency at the lower static magnetic field. This approach is termed the *joint method* [8]. To overcome the limited possible pairs of static magnetic fields available with existing NMR spectrometers, we developed a strategy that interpolates the data sets for any two static fields to obtain a third data set that can be paired with a fourth experimental data set. In this paper, we demonstrate this combined field-pairing and interpolated analysis, termed the *joint-interpolated method*, by obtaining relaxation rate data sets using a 400 MHz/800 MHz spectrometer pair and a 450 MHz/ 900 MHz spectrometer pair and analyzing them globally. In this scenario, the 450 MHz data set was interpolated from data sets originating from the 400 MHz and 500 MHz spectrometer pair. In total, this analysis yields spectral density values at seven frequencies, $\omega/2\pi$: 0, 61.4, 69.1, 122.8, 138.2, 245.6, and 276.4 MHz with increased statistical degrees of freedom for subsequent model evaluation.

The different approaches for spectral density mapping were tested using relaxation data acquired for the *E. coli* ribonuclease H (RNase H) U-[^{2}H, ^{15}N] ILV (Ile δ, Ile γ2, Leu δ1, Leu δ2, Val γ1, Val γ2) [$^{13}CH_2D$] sample. RNase H (EC 3.1.26.4) is a conserved endonuclease responsible for cleaving the RNA strand of DNA/RNA hybrids in various biological processes, including reverse transcription of the viral genome in retroviral reverse transcriptases and Okazaki fragment processing during the DNA replication of the lagging strand [17]. RNase H also belongs to a broader superfamily of nucleotidyl-transferases with conserved structure and mechanism, including retroviral integrases, Holliday junction resolvases, and transposases [18, 19]. RNase H has also been the subject of many investigations in folding, structure, and dynamics [20–22].

2. Methods

2.1. Sample Preparation

Isotopically labeled RNase H was produced by transformation of BL21(DE3) with a pAED4 plasmid encoding the *E. coli* ribonuclease HI gene. Bacterial cultures were grown in M9 minimal media containing 99% ^2H_2O, ^{15}N-ammonium chloride, and $^2H_7$-glucose to OD_{600} = 0.7 before induction with 0.5 mM IPTG. Selective $^{13}CH_2D$ group labeling was achieved by supplementing the minimal growth media with 50 mg/mL of 2-ketobutyric acid-4-^{13}C,4-d_1(99% ^{13}C, 97% ^{2}H, Isotec, Sigma Aldrich) and 80 mg/mL of 2-keto-3-(methyl-^{13}C,d_1)-butyric acid-3,4,4,4-d_4 (99% ^{13}C, 98% ^{2}H, Isotec, Sigma Aldrich) an hour before induction [23, 24]. Protein expression was allowed to proceed for 4 hours at 37° C. RNase H was purified as described previously [25–27].

2.2 NMR Spectroscopy

NMR samples contained 500 μM RNase H, 100 mM $^2H_3$-sodium acetate, pH = 5.5, and 99% ^2H_2O in a 5 mm Shigemi NMR tube. Relaxation experiments were acquired at 9.4 T (400 MHz for ^{1}H spins) on a Varian Inova spectrometer with a room temperature probe and

at 11.75 T (500 MHz), 16.45 T (700 MHz), 18.8 T (800 MHz), and 21.1 T (900 MHz) on Bruker *AVANCE* spectrometers with triple-resonance *z*-axis gradient CryoProbes. The static magnetic field strengths correspond to ^{2}H Larmor frequencies of $\omega_D/2\pi$ = 61.4, 76.8, 107.4, 122.8, and 138.2 MHz. Calibration of sample temperature to 298 K was accomplished using 98% $^2H_4$-methanol [28] and small variations between spectrometers adjusted by matching chemical shifts. Relaxation rate constants R_1, $R_{1\rho}$, R_Q, R_{AP} were measured at five static B_0 fields using a modified pulse sequence with non-constant time ^{13}C chemical shift evolution in the indirect dimension [7]. The double-quantum relaxation rate constant requires correction for interactions with remote spins and was not utilized in the present work. For all four ^{2}H relaxation experiments, spectra were recorded with 32 scans per t_1 increment and 1024 × 200 complex points for $t_2 \times t_1$. Spectral width for all relaxation experiments was 12 ppm × 20 ppm ($t_2 \times t_1$). The carriers for ^{1}H and ^{13}C were set to 4.70 ppm and 15.0 ppm, respectively. Relaxation delays were set to {1 ms, 10 ms, 20 ms, 30 ms, 40 ms, 50 ms} for measurement of ^{2}H R_1 and R_Q, {1 ms, 4 ms, 8 ms, 12 ms, 16 ms, 20 ms} for measurement of ^{2}H R_{AP}, and {0.5 ms, 3 ms, 5 ms, 10 ms, 15 ms, 20 ms} for measurement of ^{2}H $R_{1\rho}$. Two or three duplicate measurements within each relaxation delay series were recorded for purposes of error estimation.

2.3 Data Processing, Assignment, and Determination of Relaxation Parameters

NMR spectra were processed using NMRPipe [29]. Identification of ^{1}H-^{13}C methyl correlations from a ^{1}H-^{13}C HSQC experiment utilized previously published *E. coli* ribonuclease HI chemical shift assignments [21, 30]. In all, 48 methyl peaks were observed: 7 Ile, 20 Leu, and 21 Val. An equivalent number of peaks was also observed for the shortest relaxation delay in each of the four ^{2}H relaxation experiments. Spectra were visualized in Sparky [31] and peak heights determined at assigned peak positions. The unweighted peak intensities were fit to mono-exponential decay functions using the trust-region non-linear least-squares algorithm implemented in the MATLAB (version R2016b) exponential library model ‘exp1’. Uncertainties in fitted relaxation rate constants were determined by Monte Carlo simulations, using estimates of Gaussian noise obtained from variation in duplicate measurements, and by jackknife simulations. The larger of the two error estimates was used as the experimental uncertainty for subsequent spectral density mapping.

2.4 Deuterium Spectral Density Mapping

The ^{2}H spin relaxation rate constants are given by [32]:

$$R_1 = 3\xi^2[J(\omega_D) + 4J(2\omega_D)] \quad (1)$$

$$R_{1\rho} = (\frac{3\xi^2}{2})[3J(0) + 5J(\omega_D) + 2J(2\omega_D)] \quad (2)$$

$$R_Q = 9\xi^2[J(\omega_D)] \quad (3)$$

$$R_{AP} = (\frac{3\xi^2}{2})[3J(0) + J(\omega_D) + 2J(2\omega_D)] \quad (4)$$

in which:

$$\xi = \frac{\pi e^2 qQ}{2h} \quad (5)$$

e is the charge on the electron, eq is the principal value of the electric field gradient tensor, Q is the nuclear quadrupole moment, h is Planck's constant, and e^2Qq/h is taken to be 167 kHz. $J(\omega)$ is the spectral density function at frequency ω, and ω_D is the ^{2}H Larmor frequency. The following sections describe three methods of calculating the spectral density values from relaxation rate constants measured at more than one static magnetic field.

2.4.1 Independent Spectral Density Mapping—The relaxation rate constants, Eqs. 1–4, are written in matrix form as:

$$\begin{bmatrix} R_1 \\ R_{1\rho} \\ R_Q \\ R_{AP} \end{bmatrix} = 3\xi^2 \begin{bmatrix} 0 & 1 & 4 \\ 3/2 & 5/2 & 1 \\ 0 & 3 & 0 \\ 3/2 & 1/2 & 1 \end{bmatrix} \begin{bmatrix} J(0) \\ J(\omega_D) \\ J(2\omega_D) \end{bmatrix} \quad (6)$$

and constitute an overdetermined system of linear equations. In the *independent method*, Eq. 6 is solved by least-squares methods (*vide infra*) to obtain values of $J(0)$, $J(\omega_D)$, and $J(2\omega_D)$ at each static magnetic field [8, 15]. Thus, relaxation rates collected at ^{2}H frequencies of 61.4, 76.8, 122.8, and 138.2 MHz were independently analyzed using Eq. 6 to generate the spectral densities for this method. At each of the four static magnetic fields, three spectral density values are derived from four relaxation rate constants, giving one degree of freedom per field or a total of four degrees of freedom. The four values of $J(0)$ obtained for each methyl group were averaged, as were the values of $J(2\omega_D) = J(122.8)$ obtained from data acquired at 9.4 T (400 MHz for ^{1}H spins) and $J(\omega_D) = J(122.8)$ obtained from data acquired at 18.8 T (800 MHz). Thus, this analysis yields values for $J(\omega)$ at eight frequencies: $J(0)$, $J(61.4)$, $J(76.8)$, $J(122.8)$, $J(138.2)$, $J(153.6)$, $J(245.6)$, and $J(276.4)$, in which the frequencies are given as $\omega/(2\pi)$ in units of MHz.

2.4.2 Joint Spectral Density Mapping—In the second approach [8], relaxation data acquired at multiple static magnetic fields are analyzed jointly to take into account any

spectral density values that contribute to the relaxation rate constants at more than one static field. In the present case, all data sets share a common value of $J(0)$ and in addition, $J(2\omega_D)$, for data acquired at 9.4 T is identical to $J(\omega_D)$ for data acquired at 18.8 T. The resulting matrix equation is:

$$\begin{bmatrix} \hat{R}_{61.4} \\ \hat{R}_{76.8} \\ \hat{R}_{122.8} \\ \hat{R}_{138.2} \end{bmatrix} = 3\xi^2 \begin{bmatrix} V & W & 0 & X & 0 & 0 & 0 & 0 \\ V & 0 & W & 0 & 0 & X & 0 & 0 \\ V & 0 & 0 & W & 0 & 0 & X & 0 \\ V & 0 & 0 & 0 & W & 0 & 0 & X \end{bmatrix} \begin{bmatrix} J(0) \\ J(61.4) \\ J(76.8) \\ J(122.8) \\ J(138.2) \\ J(153.6) \\ J(245.6) \\ J(276.4) \end{bmatrix} \quad (7)$$

in which $\hat{\mathbf{R}}_i = [R_{1,i}, R_{1\rho,i}, R_{Q,i}, R_{AP,i}]^T$, $\mathbf{V} = [0,3/2,0,3/2]^T$, $\mathbf{W} = [1,5/2,3,1/2]^T$, $\mathbf{X} = [4,1,0,1]^T$, and $\mathbf{0}$ is a 4×1 zero-matrix. The least-squares solution of Eq. 7 yields values for $J(\omega)$ at eight frequencies and no post-analysis averaging of common values is needed. Eight spectral density values are derived from 16 relaxation rate constants, consequently with eight degrees of freedom.

2.4.3 Joint-Interpolated Spectral Density Mapping—The *joint method* shown in Eq. 7 links relaxation data acquired at 9.4 T (400 MHz) and 18.8 T (800 MHz), fields that differ by a factor of two. The *joint-interpolated method* uses the data acquired at 9.4 T (400 MHz) and 11.7 T (500 MHz) to interpolate values of the relaxation rate constants at 10.55 T (450 MHz). The interpolated relaxation rate constants are then paired with the relaxation data acquired at 21.1 T (900 MHz) for joint analysis.

The normalized correlation function for reorientation of the C-D bond vector is described as [33, 34]:

$$C(t) = \frac{1}{5} e^{-\frac{t}{\tau_m}} \left(S^2 + \sum\nolimits_i a_i e^{-\frac{t}{\tau_{e,i}}} \right) \quad (8)$$

in which τ_m is the overall rotational correlation time, S^2 is the generalized order parameter, and a_i and $\tau_{e,i}$ are the amplitude and time constant for the ith term in the internal correlation function. Taking the real part of the Fourier transform of $C(t)$ yields the spectral density function:

$$J(\omega) = \frac{2}{5} \left\{ \frac{S^2 \tau_m}{1 + \omega^2 \tau_m^2} + \sum \frac{a_i \tilde{\tau}_i}{1 + \omega^2 \tilde{\tau}_i^2} \right\} \quad (9)$$

in which:

$$\tilde{\tau}_i = \left(\frac{1}{\tau_m} + \frac{1}{\tau_{e,i}}\right)^{-1} \quad (10)$$

If $\omega^2\tau_m^2 \gg 1$ and $\tau_{e,i} \ll \tau_m$, the spectral density function reduces to:

$$J(\omega) \approx \frac{2}{5}\left\{\frac{S^2}{\omega^2\tau_m} + \sum_i a_i\tilde{\tau}_i\right\} \quad (11)$$

which is a linear function of ω^{-2}. With this insight, a first-order Taylor series approximation of a given relaxation rate constant with respect to ω^{-2} yields:

$$R_{m,\omega_{D2}} \approx R_{m,\omega_{D1}} + (R_{m,\omega_{D2}} - R_{m,\omega_{D1}})\left(\frac{1}{\omega_{D2}^2} - \frac{1}{\omega_{D1}^2}\right) \quad (12)$$

$$R_{m,\omega_{D2}} \approx R_{m,\omega_{D3}} + (R_{m,\omega_{D2}} - R_{m,\omega_{D3}})\left(\frac{1}{\omega_{D2}^2} - \frac{1}{\omega_{D3}^2}\right) \quad (13)$$

in which $R_{m,\omega_{Dj}}$ is a relaxation rate constant $m = \{R_1, R_{1\rho}, R_Q, R_{AP}\}$ at a static magnetic field with ^{2}H Larmor frequency ω_{Dj}. Averaging Eqs. 12 and 13 yields an interpolation formula for relaxation rate constants at a field for which experimental values are unavailable:

$$R_{m,\omega_{D2}} \approx \frac{R_{m,\omega_{D1}} + R_{m,\omega_{D3}}}{2} + (R_{m,\omega_{D1}} - R_{m,\omega_{D3}})\frac{2\omega_{D2}^{-2} - \omega_{D1}^{-2} - \omega_{D3}^{-2}}{2(\omega_{D1}^{-2} - \omega_{D3}^{-2})} \quad (14)$$

Based on this derivation, relaxation rate constants at 10.55 T ($\omega_D/(2\pi)$ = 69.1 MHz) are estimated from data recorded at 9.4 T (61.4 MHz) and 11.74 T (76.8 MHz) using:

$$R_{m,69.1} = \frac{R_{m,61.4} + R_{m,76.8}}{2} + (R_{m,61.4} - R_{m,76.8})\frac{2\times 69.1^{-2} - 61.4^{-2} - 76.8^{-2}}{2\times(61.4^{-2} - 76.8^{-2})} \quad (15)$$

which can be expressed as:

$$R_{m,69.1} = R_{m,61.4}\left(\frac{1}{2} + \kappa\right) + R_{m,76.8}\left(\frac{1}{2} - \kappa\right) \quad (16)$$

in which:

$$\kappa = \frac{2 \times 69.1^{-2} - 61.4^{-2} - 76.8^{-2}}{2 \times (61.4^{-2} - 76.8^{-2})} \quad (17)$$

In matrix form, the relationship between the relaxation rate constants at the three static magnetic fields becomes:

$$\begin{bmatrix} R_{m,61.4} \\ R_{m,76.8} \end{bmatrix} = \begin{bmatrix} 1 & 0 \\ -\frac{1+2\kappa}{1-2\kappa} & \frac{2}{1-2\kappa} \end{bmatrix} \begin{bmatrix} R_{m,61.4} \\ R_{m,69.1} \end{bmatrix} \quad (18)$$

Consequently, for relaxation rates collected at deuterium frequencies of 61.4, 76.8, 122.8, and 138.2 Hz:

$$\begin{bmatrix} \hat{\boldsymbol{R}}_{\mathbf{61.4}} \\ \hat{\boldsymbol{R}}_{\mathbf{76.8}} \\ \hat{\boldsymbol{R}}_{\mathbf{122.8}} \\ \hat{\boldsymbol{R}}_{\mathbf{138.2}} \end{bmatrix} = 3\xi^2 \begin{bmatrix} \boldsymbol{I} & \mathbf{0} & \mathbf{0} & \mathbf{0} \\ \mathbf{0} & \boldsymbol{I} & \mathbf{0} & \mathbf{0} \\ -\frac{1+2\kappa}{1-2\kappa}\boldsymbol{I} & \mathbf{0} & \frac{2}{1-2\kappa}\boldsymbol{I} & \mathbf{0} \\ \mathbf{0} & \mathbf{0} & \mathbf{0} & \boldsymbol{I} \end{bmatrix} \begin{bmatrix} \boldsymbol{Y} & \boldsymbol{Z} & \mathbf{0} \\ \boldsymbol{Y} & \mathbf{0} & \boldsymbol{Z} \end{bmatrix} \begin{bmatrix} J(0) \\ J(61.4) \\ J(122.8) \\ J(245.6) \\ J(69.1) \\ J(138.2) \\ J(276.4) \end{bmatrix} \quad (19)$$

in which:

$$\boldsymbol{Y} = \begin{bmatrix} 0 \\ 3/2 \\ 0 \\ 3/2 \\ 0 \\ 3/2 \\ 0 \\ 3/2 \end{bmatrix} \quad \boldsymbol{Z} = \begin{bmatrix} 1 & 4 & 0 \\ 5/2 & 1 & 0 \\ 3 & 0 & 0 \\ 1/2 & 1 & 0 \\ 0 & 1 & 4 \\ 0 & 5/2 & 1 \\ 0 & 3 & 0 \\ 0 & 1/2 & 1 \end{bmatrix} \quad (20)$$

and **0** and **I** are 4-dimensional zero and identity matrices, respectively. Equation 19 is the main theoretical result of the present work. The solution of Eq. 19 yields values of the spectral density function at seven frequencies, consequently with nine degrees of freedom.

For each of the three spectral density mapping methods, spectral density values were obtained from the relaxation rates R_1, $R_{1\rho}$, R_Q, and R_{AP} measured at deuterium frequencies 61.4, 76.8, 122.8, and 138.2 MHz by solving Eqs. 6, 7, or 19 by singular value decomposition. Uncertainties in the spectral density values were obtained from the covariance matrix.

2.5. Model-Free Analysis

Spectral density values obtained by the *independent*, *joint*, and *joint-interpolated* methods were fit with the Lipari-Szabo model-free spectral density function [8, 33]:

$$J(\omega) = \frac{2}{5}\left(\frac{\frac{1}{9}S^2_{axis}\tau_m}{1+\omega^2\tau_m^2} + \frac{\left(1-\frac{1}{9}S^2_{axis}\right)\tau}{1+\omega^2\tau^2}\right) \quad (21)$$

in which S^2_{axis} is the generalized order parameter for a unit vector oriented along the symmetry axis of the methyl group, the factor of 1/9 accounts for (assumed rapid) rotation of the methyl group, and $\tau = (1/\tau_m + 1/\tau_e)^{-1}$. Fitting was performed by minimizing

$$\chi^2 = \sum_{k=1}^{K}\left[\frac{J(\omega_k) - \hat{J}(\omega_k)}{\sigma_k}\right]^2 \quad (22)$$

in which K is the number of spectral density values being fit, σ_k are the uncertainties in spectral density values determined as described above, and $\hat{J}(\omega_k)$ is the fitted value of the spectral density function. Minimization was performed using weighted non-linear least-squares in MATLAB. Uncertainties in fitted model-free parameters were obtained from Monte Carlo simulations. Values of S^2, τ_m, and τ_e were restricted to the ranges [0, 1], [0 ns, 20 ns], and [0 ns, 20 ns], respectively. Goodness-of-fit to Eq. 21 was tested by comparing the χ^2 residual from the curve-fitting procedure for each methyl group to critical values obtained for a Bonferroni-corrected confidence level $p = \alpha/N$, where $\alpha = 0.05$ and $N = 48$ is the number of methyl groups analyzed. The critical χ^2 values for the *independent, joint, and joint-interpolated methods* are 27.8, 20.4, and 18.4, respectively.

3. Results

3.1 Simulation of 69.1 MHz Deuterium Frequency Relaxation Rate Interpolation

The accuracy of the proposed method for interpolation of relaxation rate constants necessary for the *joint-interpolated* approach was evaluated by theoretical calculations. Relaxation rates at 9.4 T, 10.55 T, and 11.7 T were calculated using Eqs. 1–4 and the Lipari-Szabo model-free formalism, Eq. 21. The percentage differences between the interpolated and exact values of the relaxation rate constants at 10.55 T are shown in Figure 1. The predicted rates show errors of ≤ 1% up to a τ_e of 1 ns, consistent with the experimental uncertainties in measured ^{2}H relaxation rates (~1–2%).

3.2 Model Selection

Spectral density values for each methyl resonance determined by each spectral density mapping method were fit with Eq. 21. If any of the three fits for a particular methyl group yielded a χ^2 value that was less than or equal to the respective critical χ^2 value, then that methyl group was included in subsequent comparisons between the three spectral density mapping methods. Methyl groups that did not meet this criterion were not considered

further; these methyl groups require fitting with more complex motional models than Eq. 21 [8]. Overall, 33 of the 48 ILV methyl resonances satisfied this criterion. Fits to data for Leu 103 δ1 converged poorly and yielded large errors for τ_m; consequently, this methyl group was also not considered further. Figure 2 shows the locations of ILV amino acids in RNase H. Most of the methyl groups chosen for analysis are in residues located either in α-helices or β-sheets, while the other methyl groups are typically located in dynamic loops or termini.

3.3 Representative Spectral Density Functions

Examples of the Lipari-Szabo model-free fits to the spectral density values obtained from the three spectral density mapping methods are shown in Figure 3. Values of τ_m were optimized independently for each methyl group and consequently τ_m represents an effective local correlation time and could be smaller than the global rotational correlation time of RNase H, as determined from ^{15}N spin relaxation [27]. Results are shown for Val 121 γ2, with a local correlation time of ~7 ns and Leucine 56 δ1 with a local correlation time of ~14 ns.

3.4 Accuracy and Precision of Model Free Parameters

Figure 4 summarizes the results of fitting the spectral densities to the Lipari-Szabo model-free formalism to obtain S^2_{axis}, τ_m, and τ_e for 32 methyl groups. Each graph in the figure shows a one-on-one comparison between model-free parameters determined by two of the three spectral density mapping procedures. Coefficients of determination, R^2, were calculated for each of the plots based on the $y = x$ line in Figure 4. The R^2 values were 0.99, 0.94, and 0.97, respectively, for S^2_{axis} comparisons, Figures 4a–c; 0.98, 0.93, and 0.97, respectively, for τ_m comparisons, Figures 4d–f; and 1.00 for all three τ_e comparisons, Figures 4g–i. Slopes of least-squares fitted lines were 0.99, 0.97, and 0.98, respectively, for S^2_{axis} comparisons, Figures 4a–c; 1.01, 1.02, and 1.02, respectively, for τ_m comparisons, Figures 4d–f; and 1.00 for all three τ_e comparisons, Figures 4g–i. The average uncertainties in the fitted Lipari-Szabo parameters, S^2_{axis}, τ_m, and τ_e, differed between the three methods of spectral density mapping. The *joint-interpolated* method yielded the smallest parameter uncertainties and Table 1 presents the percentage improvement in average uncertainties for this method compared with the *independent* and *joint* approaches.

3.5 Cross Validation with 700 MHz Spectrometer-Generated Data

The fitted model-free parameters were cross-validated by back-calculating relaxation rate constants expected for data acquired at 16.4 T (700 MHz, $\omega_D/(2\pi)$ = 107.5 MHz) using Eqs. 1–4 and Eq. 21 and then compared to experimental data acquired at 16.4 T. Uncertainties in back-calculated relaxation rate constants were generated by Monte Carlo simulations. The cross-validated results are shown in Figure 5. The three methods of spectral density mapping gave equally accurate back-predictions of the relaxation rate constants compared with experimental values. R_1 comparisons had R^2 values of 1.00, $R_{1\rho}$ comparisons had R^2 values of 0.99, R_Q comparisons had R^2 values of 0.99, and R_{AP} comparisons had R^2 values of 0.98. R_1 and $R_{1\rho}$ comparisons had slopes of 1.01, R_Q comparisons for *independent* and *joint*

methods had slopes of 0.99, R_Q comparison for the *joint-interpolated method* had a slope of 0.98, and R_{AP} comparisons had slopes of 1.02.

3.6 Local Diffusion Times

The values of τ_m obtained for the most rigid methyl-bearing side chains in RNase H are expected to report on the overall rotational diffusion tensor, which has been determined previously by ^{15}N spin relaxation [27]. As shown in Figure 6, the values of the local diffusion constants, $D = 1/(6\tau_m)$, for the 12 methyl groups with the largest values of τ_m (smallest values of D; shown in red) agree well with the predictions derived from the diffusion tensor obtained from ^{15}N spin relaxation. This agreement provides additional evidence for the accuracy of the proposed analysis for determination of rotational diffusion tensors of proteins, particularly in cases for which orientations of N-H amide bond vectors are not uniformly distributed [35].

3.7 Extent of Interpolation and Extrapolation

Given the success of the above method for the interpolation of relaxation rate constants necessary for the *joint-interpolated* approach, the accuracy of either interpolation or extrapolation was evaluated further by theoretical calculations and simulations that tested the bounds of Eq. 14. Relaxation rates at 9.4 T, 11.7 T, 18.8 T, and 21.1 T (corresponding to the two lowest and two highest experimentally-collected fields) were calculated using Eqs. 1–4 and the Lipari-Szabo model-free formalism, Eq. 21, with set values for the input variables. Four separate simulations were conducted as shown in Figure 7. Relaxation rate constants were interpolated for methyl frequencies between $\omega_D/(2\pi)$ = 61.4 MHz – 76.8 MHz (Fig. 7a) and extrapolated for relaxation rate constants for methyl frequencies below $\omega_D/(2\pi)$ = 61.4 MHz using the $\omega_D/(2\pi)$ = 61.4 and 76.8 MHz pair of relaxation rate constants (Fig. 7b). Relaxation rate constants were interpolated for methyl frequencies between $\omega_D/(2\pi)$ = 107.4 MHz – 138.2 MHz (Fig. 7c) and extrapolated for methyl frequencies above $\omega_D/(2\pi)$ = 138.2 MHz (Fig. 7d) for the $\omega_D/(2\pi)$ = 107.4 MHz and 138.2 MHz pair of relaxation rate constants.

Percentage differences between the interpolated/extrapolated and exact values of the relaxation rate constants are shown in Figure 7. The $R_{1\rho}$ and R_{AP} relaxation rate constants generally have smaller percentage errors compared to R_1 and R_Q, likely because the $J(0)$ contributions to Eqs. 2 and 4 remain constant regardless of method of calculation. Given that the experimental uncertainties in measured ^{2}H relaxation rates range from ~1–2%, extrapolation or interpolation of relaxation rate constants is generally accurate for methyl frequencies that are within ~15 MHz of one of the given pair of available measurements.

The interpolation results shown in Fig. 7d were tested experimentally by using the experimental data recorded for values of $\omega_D/(2\pi)$ = 107.4 MHz and 138.2 MHz to interpolate values of relaxation rate constants for $\omega_D/(2\pi)$ = 122.8 MHz. Figure 8 compares the interpolated and measured values of the relaxation rate constants at 122.8 MHz. The root-mean-square percentage deviations between the predicted and measured relaxation rate constants are very similar to the measured experimental uncertainties in the measured rate

constants, consistent with the predictions of Fig. 7d and further confirming the accuracy of the proposed method of interpolation.

4. Discussion and Conclusion

NMR spin relaxation methods are powerful approaches for characterizing conformational dynamics of biological macromolecules. Weaknesses of these methods are that the target spectral density function can only be sampled at the discrete eigenfrequencies of the spin system being studied and that model spectral density functions can have many optimizable parameters. Both of these weaknesses are alleviated by acquiring additional relaxation data at multiple static magnetic fields [36].

The present work examined three methods of performing spectral density mapping of ^{2}H relaxation in $^{13}CH_2D$ methyl group isotopomers, which have been termed *independent*, *joint*, and *joint-interpolated*. The latter two approaches make use of a unique feature of ^{2}H quadrupolar relaxation: the number of spectral density values entering into the relaxation equations is reduced if data are acquired at pairs of static magnetic fields that differ by a factor of two. As relatively few such paired fields are available at present (in the current work, only 400 MHz/800 MHz), the *joint-interpolation method* approximates such pairings, in the current work by interpolating between 400 MHz and 500 MHz to generate relaxation data at 450 MHz for pairing with 900 MHz data. The major advantages of the *joint* and *joint-interpolation methods* are the consequent additional increases in the statistical degrees of freedom compared with the *independent method*.

Comparisons among the three spectral density mapping methods and cross validation with an independent data set indicated that the three approaches were equally accurate; however, the joint-interpolation method yielded an improvement in precision for the final fitted model-free parameters of between 10–15% compared to the *independent method* and of between 7–11% compared with the *joint* analysis. These results would make the *joint-interpolation method* preferable over the other two methods. Notably, no additional data need to be acquired to implement the *joint-interpolated* method and as more commercial NMR spectrometers with frequencies of 1000 MHz and 1200 MHz become available, additional pairs of fields become accessible, further increasing the power of this method.

Acknowledgments

This work was supported by National Institutes of Health grant R01 GM059273 (A. G. P.) and T32 GM008281 (A. H. and P. A. O). Some of the work presented here was conducted at the Center on Macromolecular Dynamics by NMR Spectroscopy located at the New York Structural Biology Center, supported by a grant from the NIH National Institute of General Medical Sciences (P41 GM118302). A.G.P. is a member of the New York Structural Biology Center. The data collected at NYSBC was made possible by a grant from NYSTAR and ORIP/NIH facility improvement grant CO6RR015495. The 700 MHz spectrometer was purchased with funds from NIH grant S10OD018509. The 900 MHz NMR spectrometers were purchased with funds from NIH grant P41GM066354, the Keck Foundation, New York State Assembly, and U.S. Dept. of Defense.

References

1. Nussinov R, Jang H, Tsai CJ, Liao TJ, Li S, Fushman D, Zhang J. Intrinsic protein disorder in oncogenic KRAS signaling. Cell. Mol. Life Sci. 2017; 74:3245–3261. [PubMed: 28597297]

2. Csizmok V, Follis AV, Kriwacki RW, Forman-Kay JD. Dynamic protein interaction networks and new structural paradigms in signaling. Chem. Rev. 2016; 116:6424–6462. [PubMed: 26922996]
3. Dethoff EA, J C, Mustoe AM, Al-Hashimi HM. Functional complexity and regulation through RNA dynamics. Nature. 2012; 482:322–330. [PubMed: 22337051]
4. Palmer AG. NMR characterization of the dynamics of biomacromolecules. Chem. Rev. 2004; 104:3623–3640. [PubMed: 15303831]
5. Kay LE. New views of functionally dynamic proteins by solution NMR spectroscopy. J. Mol. Biol. 2016; 428:323–331. [PubMed: 26707200]
6. Narayanan C, Bafna K, Roux LD, Agarwal PK, Doucet N. Applications of NMR and computational methodologies to study protein dynamics. Arch. Biochem. Biophys. 2017; 628:71–80. [PubMed: 28483383]
7. Millet O, Muhandiram DR, Skrynnikov NR, Kay LE. Deuterium spin probes of sidechain dynamics in proteins. 1. Measurement of five relaxation rates per deuteron in ^{13}C-labeled and fractionally ^{2}H-enriched proteins in solution. J. Am. Chem. Soc. 2002; 124:6439–6448. [PubMed: 12033875]
8. Skrynnikov NR, Millet O, Kay LE. Deuterium spin probes of side-chain dynamics in proteins. 2. Spectral density mapping and identification of nanosecond time-scale side-chain motions. J. Am. Chem. Soc. 2002; 124:6449–6460. [PubMed: 12033876]
9. Sheppard D, Li DW, Bruschweiler R, Tugarinov V. Deuterium spin probes of backbone order in proteins: ^{2}H NMR relaxation study of deuterated carbon alpha sites. J. Am. Chem. Soc. 2009; 131:15853–15865. [PubMed: 19821582]
10. Tugarinov V, Kay LE. A ^{2}H NMR relaxation experiment for the measurement of the time scale of methyl side-chain dynamics in large proteins. J. Am. Chem. Soc. 2006; 128:12484–12489. [PubMed: 16984199]
11. Vallurupalli P, Kay LE. A suite of ^{2}H NMR spin relaxation experiments for the measurement of RNA dynamics. J. Am. Chem. Soc. 2005; 127:6893–6901. [PubMed: 15869313]
12. Vallurupalli P, Scott L, Hennig M, Williamson JR, Kay LE. New RNA labeling methods offer dramatic sensitivity enhancements in ^{2}H NMR relaxation spectra. J. Am. Chem. Soc. 2006; 128:9346–9347. [PubMed: 16848466]
13. Peng JW, Wagner G. Frequency spectrum of NH bonds in eglin c from spectral density mapping at multiple fields. Biochemistry. 1995; 34:16733–16752. [PubMed: 8527448]
14. Ishima R, Nagayama K. Quasi-spectral density function analysis for nitrogen-15 nuclei in proteins. J. Magn. Reson., Ser. B. 1995; 108:73–76.
15. Johnson E, Chazin WJ, Rance M. Effects of calcium binding on the side-chain methyl dynamics of calbindin D_{9k}: a ^{2}H NMR relaxation study. J. Mol. Biol. 2006; 357:1237–1252. [PubMed: 16476440]
16. Ishima R, Petkova AP, Louis JM, Torchia DA. Comparison of methyl rotation axis order parameters derived from model-free analyses of ^{2}H and ^{13}C longitudinal and transverse relaxation rates measured in the same protein sample. J. Am. Chem. Soc. 2001; 123:6164–6171. [PubMed: 11414851]
17. Tadokoro T, Kanaya S. Ribonuclease H: molecular diversities, substrate binding domains, and catalytic mechanism of the prokaryotic enzymes. FEBS J. 2009; 276:1482–1493. [PubMed: 19228197]
18. Nowotny M. Retroviral integrase superfamily: the structural perspective. EMBO Rep. 2009; 10:144–151. [PubMed: 19165139]
19. Moelling K, Broecker F. The reverse transcriptase-RNase H: from viruses to antiviral defense. Ann. N. Y. Acad. Sci. 2015; 1341:126–135. [PubMed: 25703292]
20. Hollien J, Marqusee S. Comparison of the folding processes of *T. thermophilus* and *E. coli* ribonucleases H. J. Mol. Biol. 2002; 316:327–340. [PubMed: 11851342]
21. Butterwick JA, Loria JP, Astrof NS, Kroenke CD, Cole R, Rance M, Palmer AG. Multiple time scale backbone dynamics of homologous thermophilic and mesophilic ribonuclease HI enzymes. J. Mol. Biol. 2004; 339:855–871. [PubMed: 15165855]
22. Katayanagi K, Miyagawa M, Matsushima M, Ishikawa M, Kanaya S, Ikehara M, Matsuzaki T, Morikawa K. Three-dimensional structure of ribonuclease H from *E. coli*. Nature. 1990; 347:306–309. [PubMed: 1698262]

23. Tugarinov V, Kanelis V, Kay LE. Isotope labeling strategies for the study of high-molecular-weight proteins by solution NMR spectroscopy. Nat. Protoc. 2006; 1:749–754. [PubMed: 17406304]
24. Tugarinov V, Ollerenshaw JE, Kay LE. Probing side-chain dynamics in high molecular weight proteins by deuterium NMR spin relaxation: an application to an 82-kDa enzyme. J. Am. Chem. Soc. 2005; 127:8214–8225. [PubMed: 15926851]
25. Yang W, Hendrickson WA, Kalman ET, Crouch RJ. Expression, purification, and crystallization of natural and selenomethionyl recombinant ribonuclease H from *Escherichia coli*. J. Biol. Chem. 1990; 265:13553–13559. [PubMed: 2199440]
26. Mandel AM, Akke M, Palmer AG. Backbone dynamics of Escherichia coli ribonuclease HI: correlations with structure and function in an active enzyme. J. Mol. Biol. 1995; 246:144–163. [PubMed: 7531772]
27. Kroenke CD, Loria JP, Lee LK, Rance M, Palmer AG. Longitudinal and transverse ^{1}H-^{15}N dipolar ^{15}N chemical shift anisotropy relaxation interference: Unambiguous determination of rotational diffusion tensors and chemical exchange effects in biological macromolecules. J. Am. Chem. Soc. 1998; 120:7905–7915.
28. Findeisen M, Brand T, Berger S. A ^{1}H-NMR thermometer suitable for cryoprobes. Magn. Reson. Chem. 2007; 45:175–178. [PubMed: 17154329]
29. Delaglio F, Grzesiek S, Vuister GW, Zhu G, Pfeifer J, Bax A. NMRPipe: a multidimensional spectral processing system based on UNIX pipes. J. Biomol. NMR. 1995; 6:277–293. [PubMed: 8520220]
30. Yamazaki T, Yoshida M, Nagayama K. Complete assignments of magnetic resonances of ribonuclease H from Escherichia coli by double- and triple-resonance 2D and 3D NMR spectroscopies. Biochemistry. 1993; 32(21):5656–5669. [PubMed: 8389189]
31. Lee W, Tonelli M, Markley JL. NMRFAM-SPARKY: enhanced software for biomolecular NMR spectroscopy. Bioinformatics. 2015; 31:1325–1327. [PubMed: 25505092]
32. Cavanagh, J., Fairbrother, WJ., Palmer, AG., Rance, M., Skelton, NJ. Protein NMR Spectroscopy: Principles and Practice. 2. Academic Press; Amsterdam; Boston: 2007.
33. Lipari G, Szabo A. Model-free approach to the interpretation of nuclear magneticresonance relaxation in macromolecules. 1. Theory and range of validity. J. Am. Chem. Soc. 1982; 104:4546–4559.
34. Lipari G, Szabo A. Model-free approach to the interpretation of nuclear magneticresonance relaxation in macromolecules. 2. Analysis of experimental results. J. Am. Chem. Soc. 1982; 104:4559–4570.
35. Lee LK, Rance M, Chazin WJ, Palmer AG. Rotational diffusion anisotropy of proteins from simultaneous analysis of ^{15}N and $^{13}C^{a}$ nuclear spin relaxation. J. Biomol. NMR. 1997; 9(287–298)
36. Gill ML, Byrd RA, Palmer AG. Dynamics of GCN4 facilitate DNA interaction: a model-free analysis of an intrinsically disordered region. Phys. Chem. Chem. Phys. 2016; 18:5839–5849. [PubMed: 26661739]

Highlights

1. ^{2}H relaxation rates for *E. coli* ribonuclease H at four static magnetic fields
2. Evaluation of three approaches for spectral density mapping of multiple field data
3. Cross validation with a fifth magnetic field establishes accuracy of all methods
4. Novel interpolation strategy improves precision of fitted model-free parameters

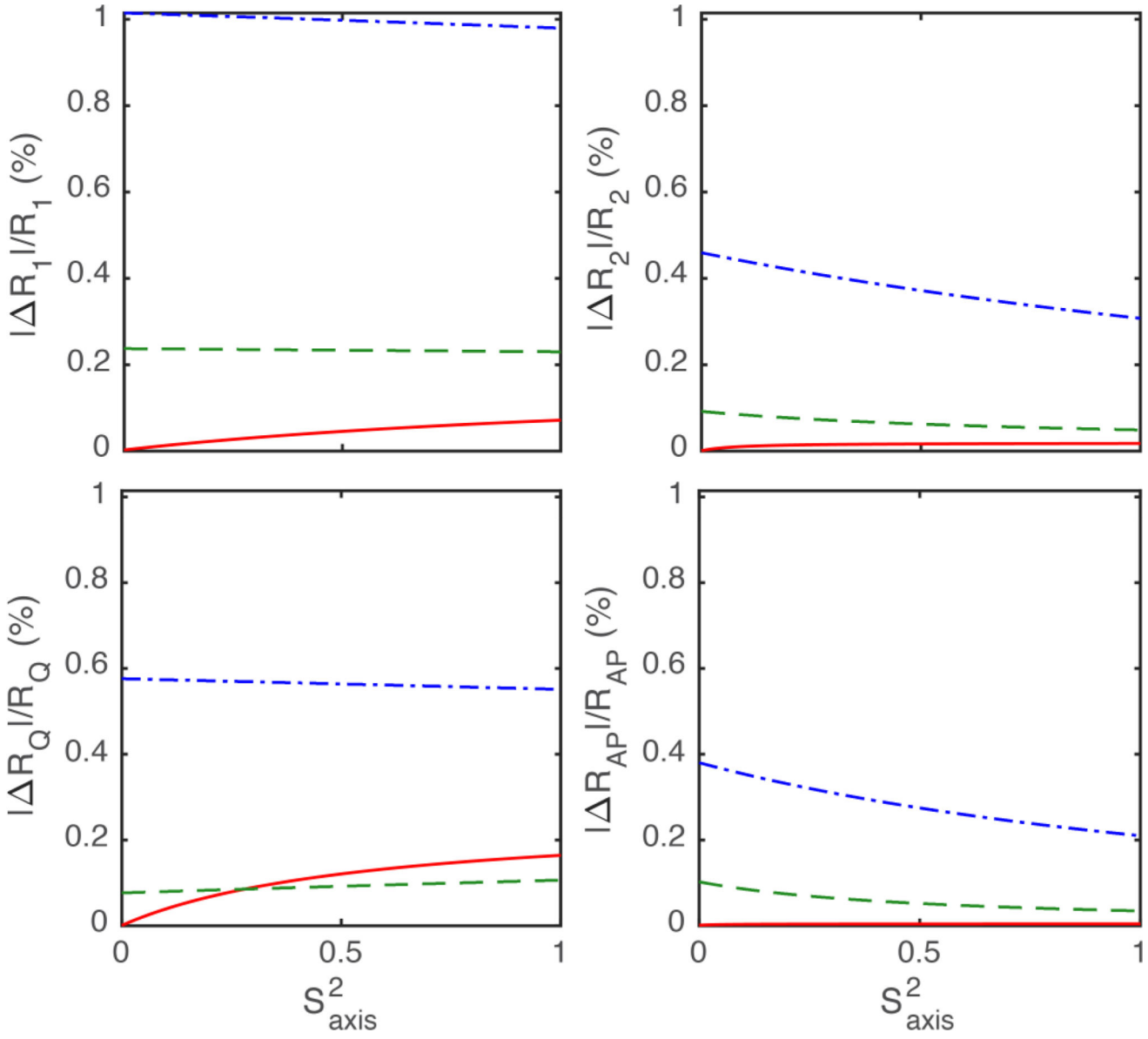

Figure 1.

Predicted errors for Eq. 16 over a range of methyl axis order parameters S^2_{axis} from 0 to 1, given an overall tumbling time τ_m of 10 nanoseconds (ns), and effective correlation times τ_e of (solid, red) 0.03 ns, (dashed, green) 0.3 ns, and (dot-dashed, blue) 1 ns.

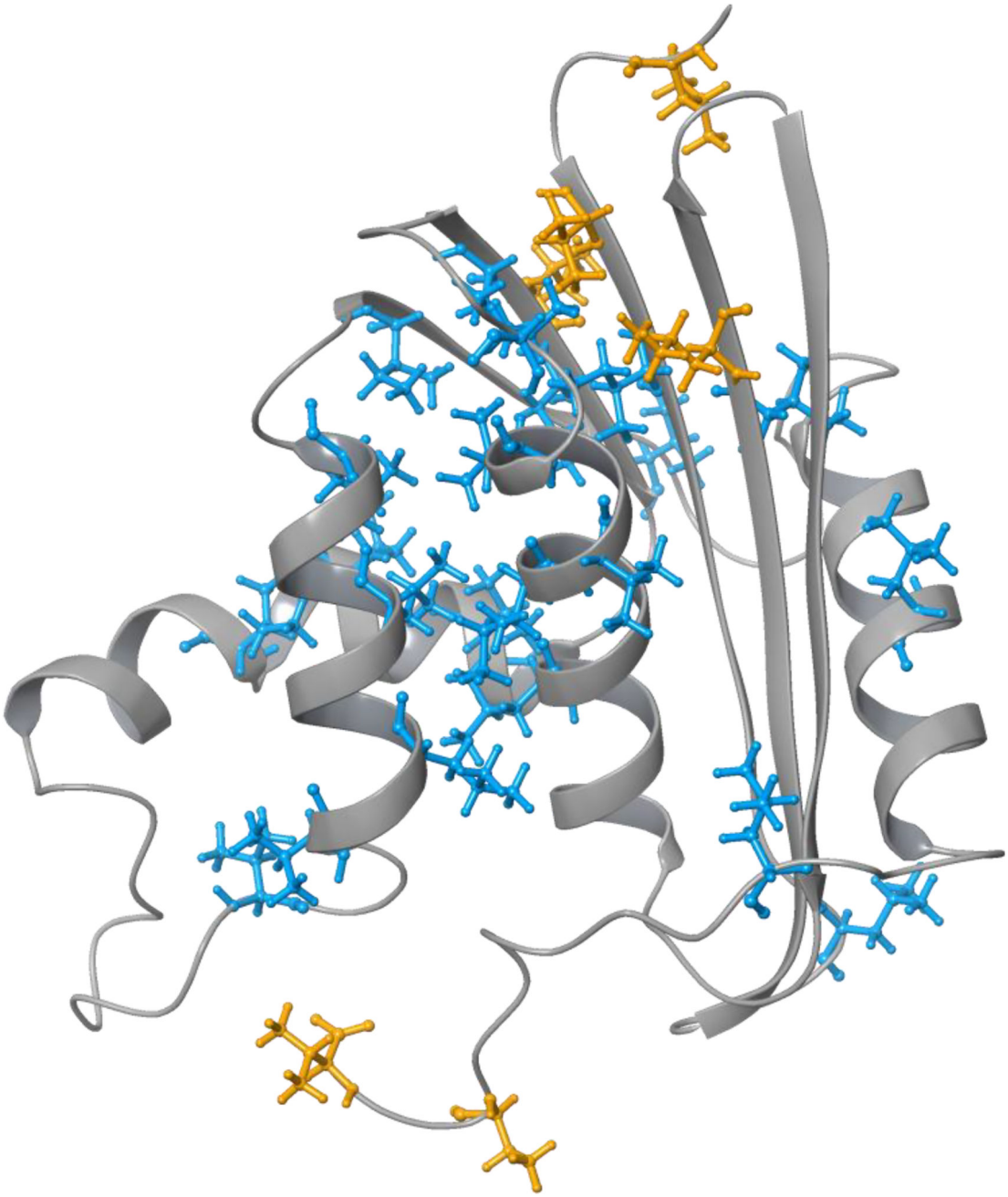

Figure 2.

Ribbon diagram of RNase H with the observable ILV residues in stick representations. The ILV residues containing methyl relaxation data fit with the Lipari-Szabo model-free formalism, Eq. 21, are colored blue; excluded ILV residues are colored orange.

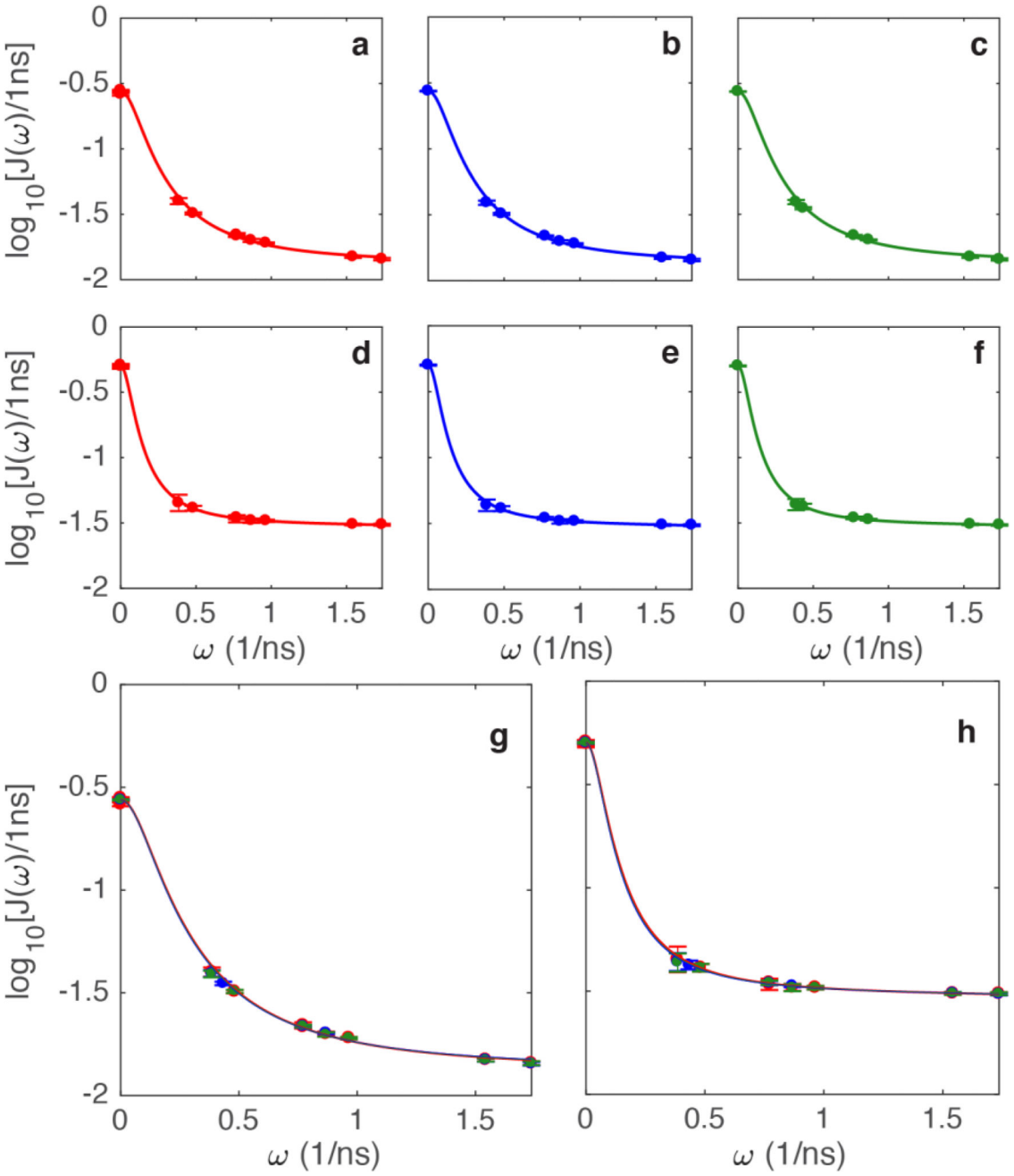

Figure 3.

(a–f) represent the individual fits for (red) *independent*, (blue) *joint*, and (green) *joint-interpolated)*. The first row *(a–c)* shows plots for Val 121 γ2, with each method, plotted individually. The second row *(d–f)* shows plots for Leu 56 δ1, with each method also plotted individually. Superposition of data and fits for the three methods are shown for (*g*) Val 121 γ2 and (*h*) Leu 56 δ1.

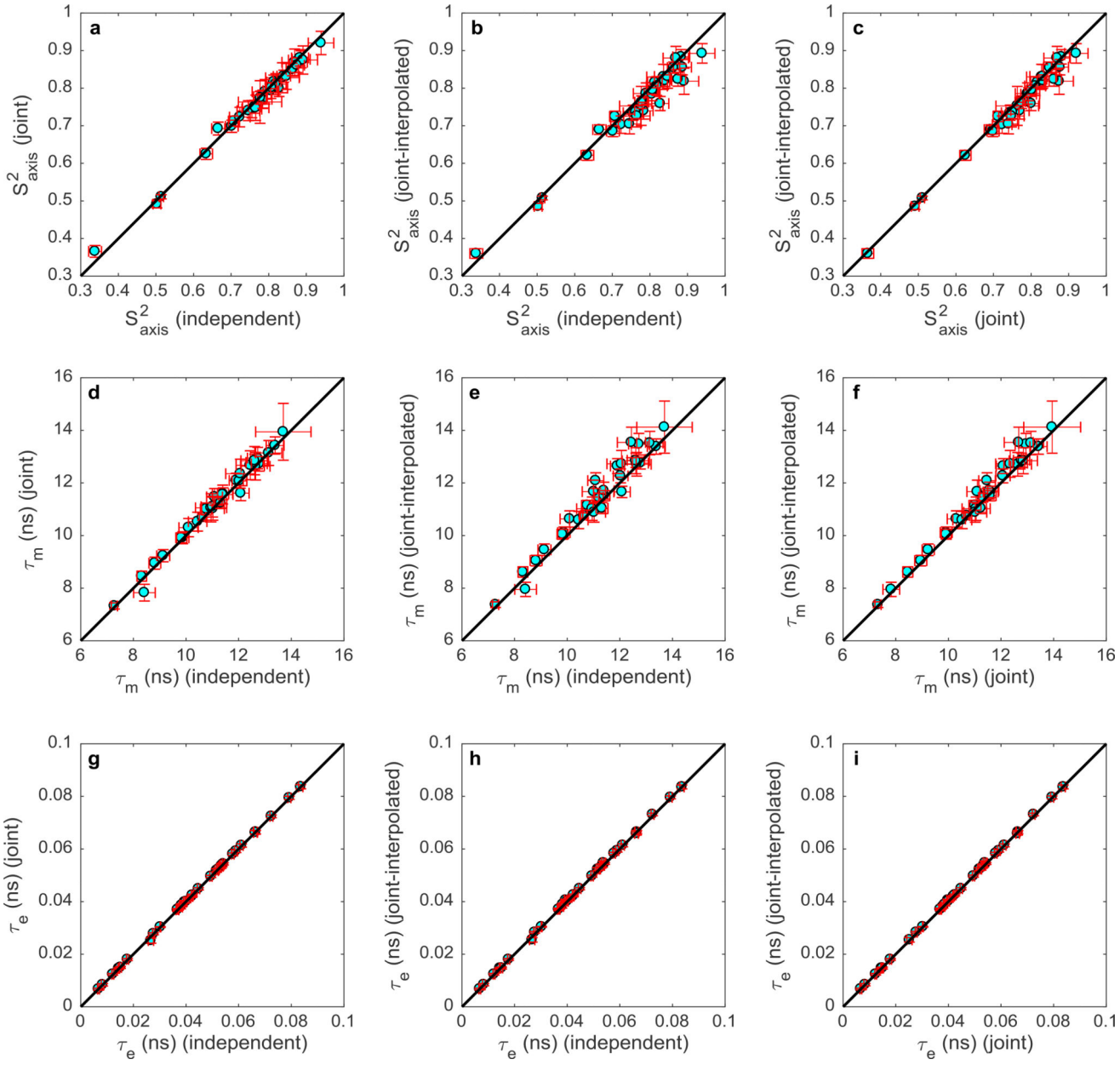

Figure 4.

Correlation plots for S^2_{axis} (top row a–c), τ_m (middle row d–f), and τ_e (bottom row g–i). Each row compares the model free parameters generated from the *independent*, *joint*, and *joint-interpolated methods*. The parameters of the 32 residues are shown in cyan, while the error bars are depicted in red. The black line represents $y=x$.

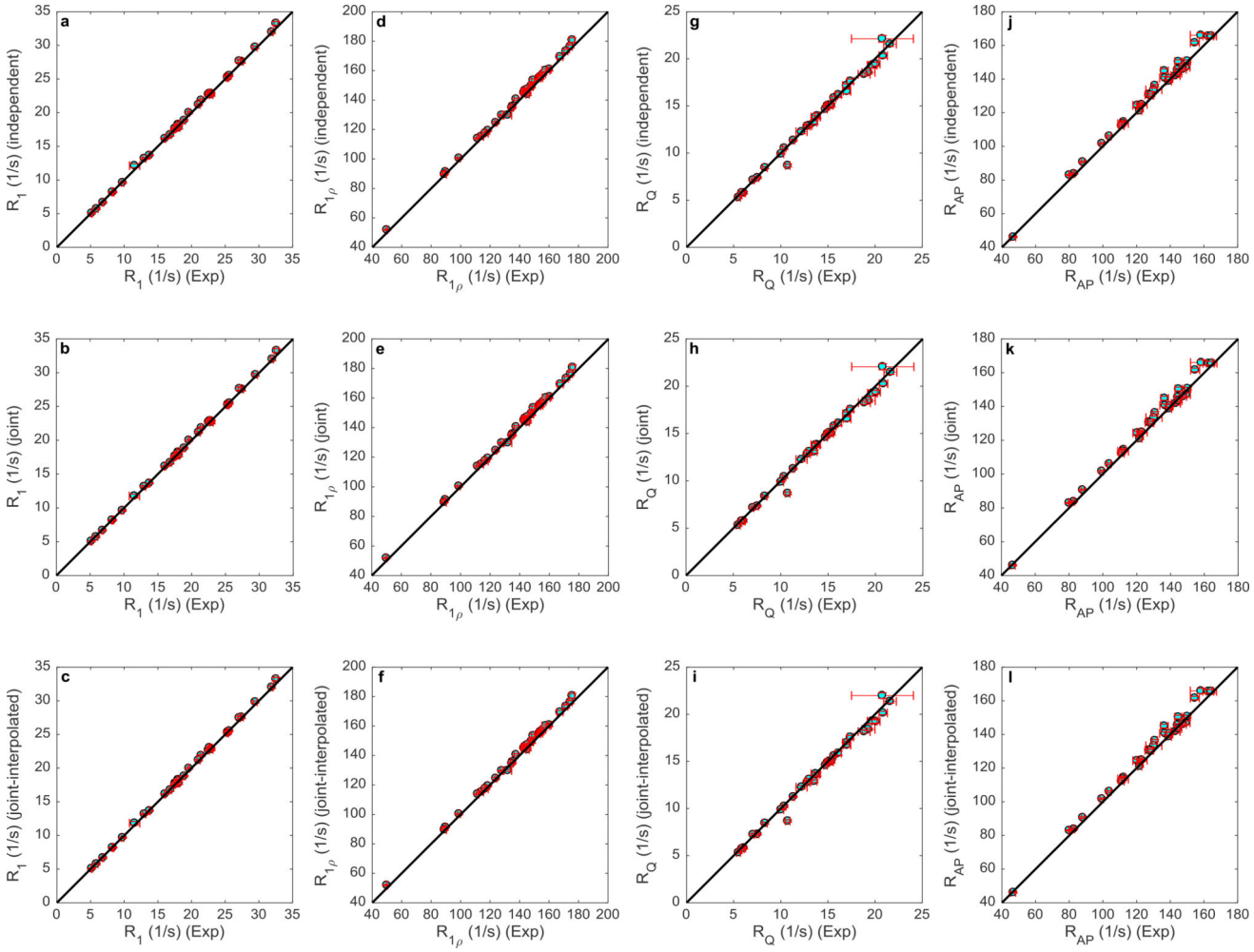

Figure 5.

Back-calculated 700 MHz relaxation rate constants (*y*-axis) are compared to the experimental results (*x*-axis). Each row represents a method of spectral density mapping, while each column represents a relaxation rate constant. The relaxation rates of the 32 residues are shown in cyan, while the error bars are depicted in red. The black line represents $y=x$.

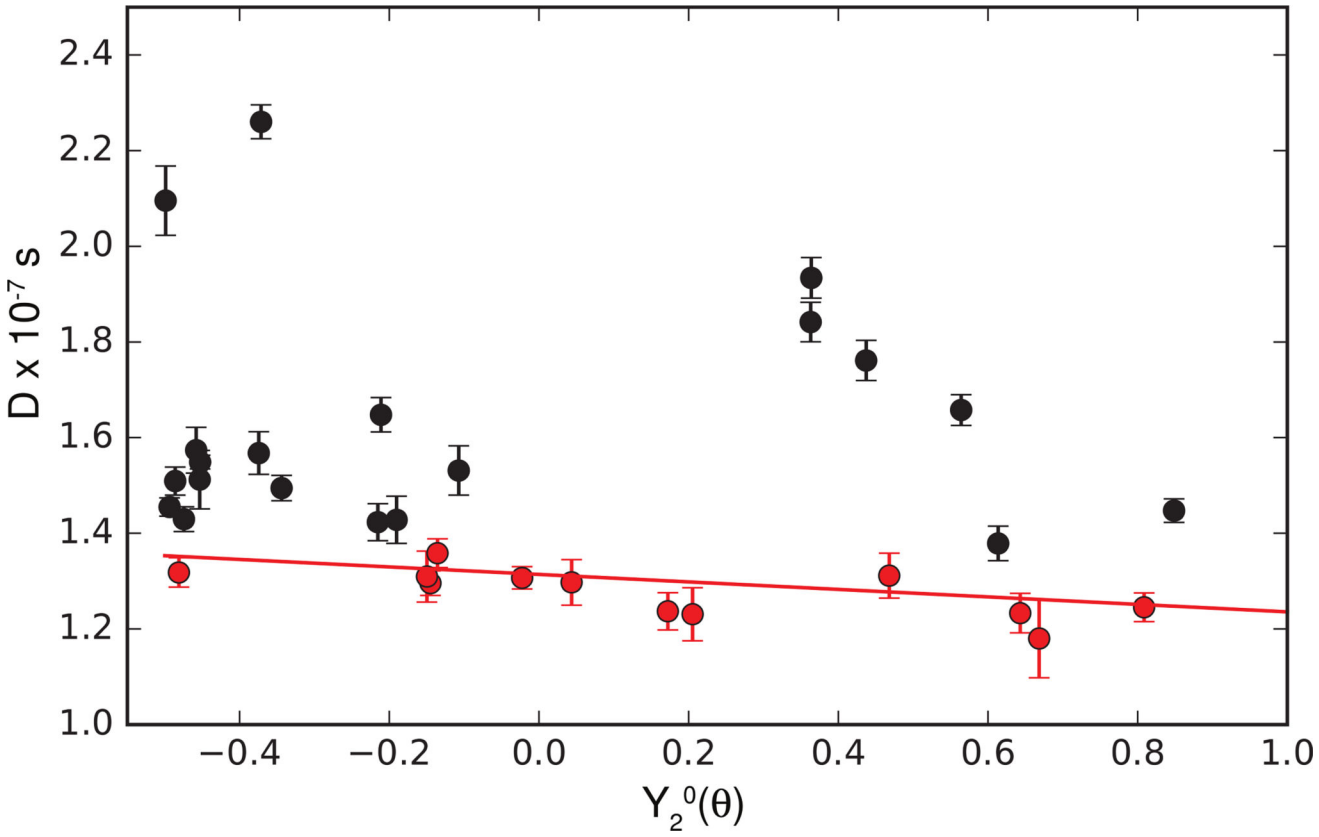

Figure 6.

Local diffusion times ($D = 1/(6\tau_m)$) plotted versus $Y_2^0(\theta)$, in which θ is the orientation of the methyl symmetry axis in the structure of RNase H oriented in the principal axis system of the diffusion tensor determined from ^{15}N spin relaxation. The values of D for the 12 slowest tumbling residues (for which internal motions are well-separated from overall rotation) are shown in red and agree quantitatively with predictions from the overall rotational diffusion tensor determined from ^{15}N relaxation data (red line), when adjusted for the sample temperature and D_2O viscosity.

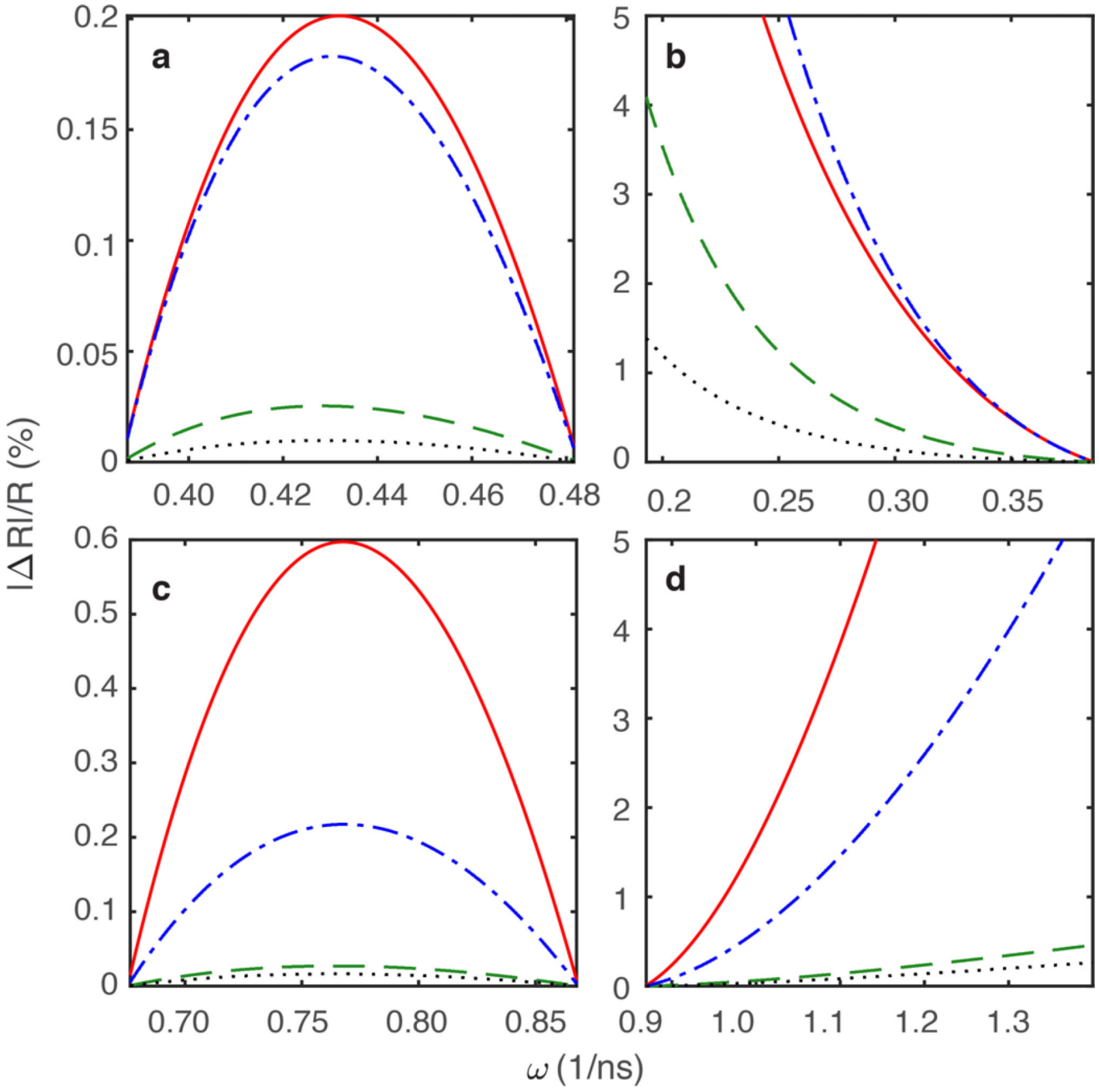

Figure 7.

Predicted errors for Eq. 14 over a range of methyl frequencies ω(1/ns), given set values of methyl axis order parameters S^2_{axis} of 0.5, overall tumbling time τ_m of 10 nanoseconds, and effective correlation times τ_e of 0.3 nanoseconds. The red solid line represents R_1, the green dashed line represents $R_{1\rho}$, the blue dot-dashed line represents R_Q, and the black dotted line represents R_{AP}. (a) Interpolated for methyl frequencies between $\omega_D/(2\pi)$ = 61.4 MHz – 76.8 MHz. (b) Extrapolated for methyl frequencies below $\omega_D/(2\pi)$ = 61.4 MHz using the $\omega_D/(2\pi)$ = 61.4 and 76.8 MHz pair of relaxation rate constants. (c) Interpolation for methyl

frequencies between $\omega_D/(2\pi)$ = 107.4 MHz – 138.2 MHz. (d) Extrapolation above $\omega_D/(2\pi)$ = 138.2 MHz for the $\omega_D/(2\pi)$ = 107.4 MHz and 138.2 MHz pair of relaxation rate constants.

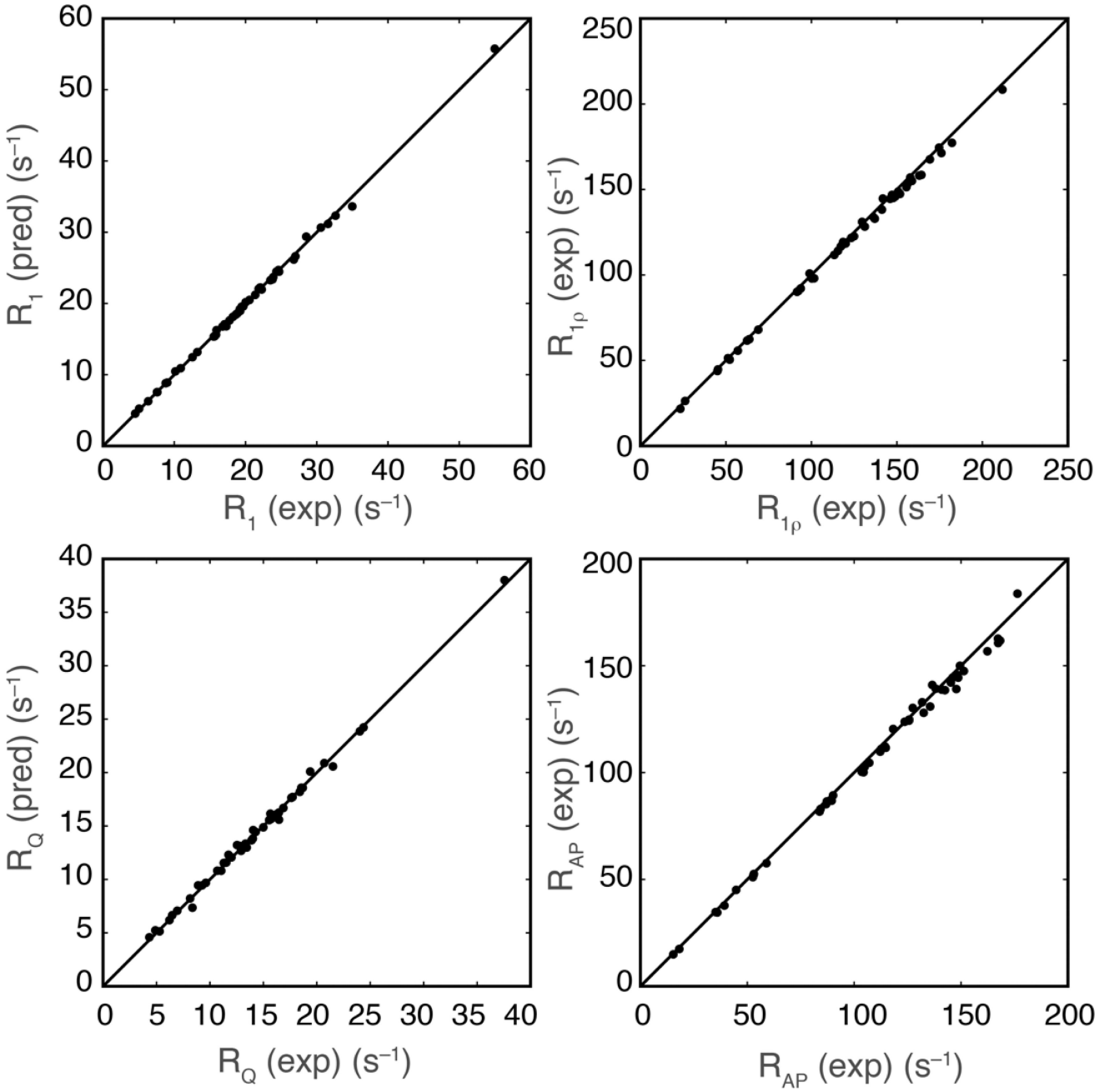

Figure 8.

Comparison of ^{2}H relaxation rate constants (pred) interpolated and (exp) measured at $\omega_D/(2\pi)$ = 122.8 MHz. Interpolation was performed using measured values of the relaxation rate constants with $\omega_D/(2\pi)$ = 107.4 MHz and 138.2 MHz. For R_1, the slope of a line fitted through the origin was 0.997, the root-mean-square (rms) relative variation was 1.0%. The rms relative uncertainty in the measured values was 1.8%. For $R_{1\rho}$, the slope of a line fitted through the origin was 0.984, the rms relative variation was 1.5%. The rms relative uncertainty in the measured values was 1.6%. For R_Q, the slope of a line fitted through the origin was 0.983, the rms relative variation was 2.2%. The rms relative uncertainty in the

measured values was 2.7%. For R_{AP}, the slope of a line fitted through the origin was 0.997, the root-mean-square percent variation was 1.9%. The rms relative uncertainty in the measured values was 2.2%. The rms relative variations between predicted and experimental values shown above were divided by $2^{1/2}$ to allow direct comparison to relative variation in experimental values.

Table 1

Improvement in precision of fitted model-free parameters

% More Precise	*Joint-Interpolated* vs. *Independent*	*Joint-Interpolated* vs. *Joint*
S^2	14.6%	10.8%
τ_m	10.5%	7.8%
τ_e	12.8%	10.1%